PHYSICAL REVIEW B **90**, 161403(R) (2014)

RKKY interaction and intervalley processes in *p*-doped transition-metal dichalcogenides

Diego Mastrogiuseppe, Nancy Sandler, and Sergio E. Ulloa

Department of Physics and Astronomy, and Nanoscale and Quantum Phenomena Institute, Ohio University, Athens, Ohio 45701–2979, USA

(Received 10 August 2014; revised manuscript received 26 September 2014; published 10 October 2014)

We study the Ruderman-Kittel-Kasuya-Yosida interaction in *p*-doped transition-metal dichalcogenides such as MoS_2 and WS_2. We consider magnetic impurities hybridized to the Mo *d* orbitals characteristic of the valence bands. Using the Matsubara Green's-function formalism, we obtain the two-impurity interaction vs their separation and chemical potential of the system, accounting for the important angular dependence which reflects the underlying triangular lattice symmetry. The inclusion of the valence-band valley at the Γ point results in a strong enhancement of the interaction. Electron-scattering processes transferring momentum between valleys at different symmetry points give rise to complex spatial oscillation patterns. Variable doping would allow the exploration of rather interesting behavior in the interaction of magnetic impurities on the surfaces of these materials, including the control of the interaction symmetry, which can be directly probed in scanning tunneling microscopy experiments.

DOI: 10.1103/PhysRevB.90.161403 PACS number(s): 75.30.Hx, 75.20.Hr, 75.75.−c, 75.70.Tj

Introduction. The Ruderman-Kasuya-Kittel-Yosida (RKKY) interaction [1–3], or indirect exchange, describes the effective coupling of two magnetic moments mediated by conduction electrons in a metal. Under certain conditions, this interaction can give rise to effects such as itinerant magnetic order and giant magnetoresistance [4–6], with important technological applications. As such, it directly impacts the field of spintronics [7], allowing information transfer between spins in a controlled manner.

The RKKY interaction depends on the dimensionality and underlying band structure of the host material. For example, in conventional two-dimensional (2D) metals, it oscillates with interimpurity separation r with a characteristic wavelength ($\approx\lambda_F/2$, half the Fermi wavelength in the host). The oscillation expresses the alternation between ferromagnetic (FM) and antiferromagnetic (AFM) coupling, decreasing as r^{-2} [8]. Remarkably, complex band structures can give rise to nonstandard behavior. In graphene, for instance, the RKKY interaction decays as r^{-3} for the charge neutral system, while more conventional behavior appears in the doped or gapped cases [9–18].

Other newly isolated two-dimensional layered crystals [19] allow one to explore even more interesting scenarios. A prominent example is given by transition-metal dichalcogenides (TMDs), a family of materials where the combination of hybridization and strong spin-orbit interaction, due to the heavy transition-metal atoms, results in a band structure with strong coupling of spin and valley degrees of freedom [20]. The RKKY interaction in TMDs has been recently characterized in particular for MoS_2 [21,22]. Parhizgar *et al.* report that the spin-spin interaction can be seen to include three different terms: Ising, *XY*, and Dzyaloshinskii-Moriya components [21], all found to decay as r^{-2}. In contrast, Hatami *et al.* finds that while the out-of-plane component decays as r^{-2}, the in-plane interaction decays as $r^{-5/2}$, a disagreement perhaps produced by their disregard of intervalley scattering [22].

These discrepancies reveal the subtleties involved in properly accounting for all relevant scattering processes that determine the final magnetic arrangement. Interestingly, processes that consider the valence-band valley centered at the Γ point, especially important when considering the *p*-doped case, have been neglected in previous studies. The Γ valley is known to lie not far removed in energy from the valleys at the Brillouin-zone corners in MoS_2 and WS_2 [23–27]. This valley plays a star role in the transition to the indirect gap behavior in bi- and multilayers of these materials.

We analyze the RKKY interaction for *p*-doped TMDs [28–33], and focus on the case of MoS_2 for which the relevant structure parameters are well known. The unavoidable contribution of the Γ valley significantly increases the overall interaction strength when the Fermi level is set to populate this valley. Moreover, it provides extra channels for electron-scattering processes, giving rise to complex spatial and energy modulation patterns for the anisotropic exchange-coupling constants. Remarkably, the inclusion of this valley allows for the possibility of isotropic and in-plane magnetic order, not possible in its absence. These behaviors are easily tunable by sweeping the Fermi level and turn out to be important for even relatively low *p*-doping levels.

Theoretical description. The basic structure of TMDs in their 2D form (elemental "monolayer") is a triangular layer of transition-metal atoms sandwiched between two triangular layers of chalcogen atoms (see Fig. 1).

The first Brillouin zone for the monolayer crystal is hexagonal [34] with two nonequivalent K_1 and K_{-1} valleys, in which most of the low-energy physics takes place. Lack of reflection symmetry along the z axis in the unit cell produces a splitting of the metal *d* orbitals, resulting in a direct gap at the K_1 and K_{-1} valleys. The high atomic number of the transition metal produces a sizable spin-orbit coupling which further splits the valence bands into two with opposite spin projection [23]. These two effects result in a strong spin-valley coupling, while spin remains a good quantum number [20].

Several recent *ab initio* calculations show that the (spin-degenerate) valence-band valley at the Γ point also contributes to the low-energy physics [23–27]. The Γ valley participates in virtual transitions even at low *p*-doping levels (or gating ranges) common in experiments [28–33].

The proposed effective low-energy Hamiltonian to describe these properties is given by

$$H_0 = \sum_{q,\tau} \psi^\dagger h_{K_\tau}(q)\psi + \sum_k \phi^\dagger h_\Gamma(k)\phi, \qquad (1)$$

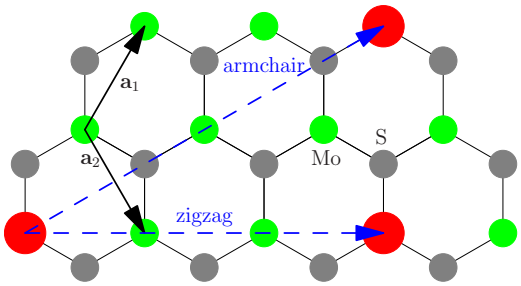

FIG. 1. (Color online) Magnetic impurities (red circles) hybridized to Mo d orbitals. Blue dashed arrows show two high-symmetry directions, i.e., zigzag and armchair, along which we compare the effective interaction between local moments. Black solid arrows indicate unit vectors.

where

$$h_{K_\tau}(q) = \begin{pmatrix} \xi & a\tau q e^{-i\tau\theta} & 0 & 0 \\ a\tau q e^{i\tau\theta} & \lambda(\tau-1) & 0 & 0 \\ 0 & 0 & \xi & a\tau q e^{-i\tau\theta} \\ 0 & 0 & a\tau q e^{i\tau\theta} & -\lambda(\tau+1) \end{pmatrix} \tag{2}$$

is the matrix near the K_τ valleys, $\tau = \pm 1$ is the valley index; $q = |\mathbf{q}|$ is the modulus of the reduced wave vector measured from K_τ, and $\theta = \arctan(q_y/q_x)$. The spinor bases are arranged as $\psi = (z^2\uparrow, xy\uparrow, z^2\downarrow, xy\downarrow)^T$, where z^2 (xy) stands for $|d_{3z^2-r^2}\rangle$ ($[|d_{x^2-y^2}\rangle + i\tau|d_{xy}\rangle]/\sqrt{2}$) Mo $3d$ orbitals, and $\phi = (p_{xy}\uparrow, d_{z^2}\uparrow, p_{xy}\downarrow, d_{z^2}\downarrow)^T$, where p_{xy} are S p_x, p_y orbitals. The up/down arrows indicate the z-spin projection. Energies are expressed throughout in units of the nearest-neighbor hopping amplitude t, a is the nearest Mo-Mo distance, $\xi = \Delta - \lambda$, where λ is the spin-orbit coupling constant, and Δ stands for the gap. Typical values for MoS_2 are $a \simeq 3.2$Å, $t \simeq 1.1$eV, so that $\Delta \simeq 1.5$, and $\lambda \simeq 0.07$. The energies have been shifted such that the top of the valence bands at the K_τ points lie at zero energy. At the Γ point, we have [26]

$$h_\Gamma(k) = E_\Gamma(k) \begin{pmatrix} 0 & 0 & 0 & 0 \\ 0 & 1 & 0 & 0 \\ 0 & 0 & 0 & 0 \\ 0 & 0 & 0 & 1 \end{pmatrix}, \tag{3}$$

where k is the modulus of the wave vector measured from the Γ point, $E_\Gamma(k) = \hbar^2 k^2/(2tm_{\text{eff}}) + \epsilon_\Gamma$. m_{eff} is the (negative) effective mass, and ϵ_Γ sets the relative position of the Γ and K_τ valleys ($\epsilon_\Gamma \approx 0.1$ in MoS_2). The conduction matrix elements were discarded due to the large gap between conduction and valence bands. A schematic representation of the valence-band structure around the three relevant points in the Brillouin zone is shown in Fig. 2(d).

Next, we consider two spin-1/2 s-wave magnetic impurities hybridized to Mo atoms, given that relevant Bloch states at low energies are composed mainly from admixtures of d orbitals from these atoms. We choose two high-symmetry directions connecting these local moments, i.e., zigzag and armchair, to show characteristic results, although many other directions are clearly possible; see Fig. 1. The interaction between each magnetic atom and conduction electron spins in the host is described by a contact interaction $H_{\text{int}} = J\sum_{j=1,2}\mathbf{S}_j \cdot \mathbf{s}(\mathbf{R}_j)$,

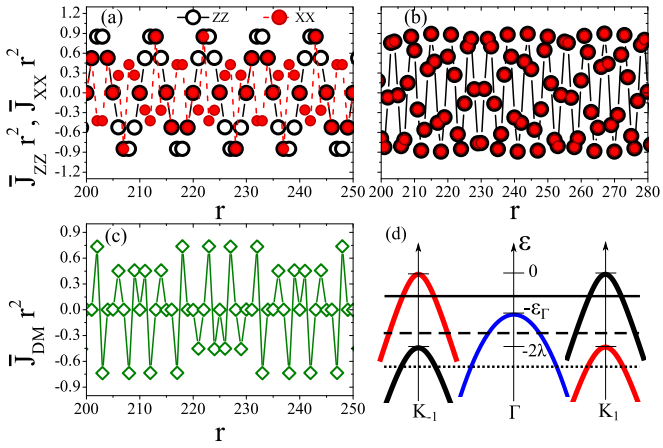

FIG. 2. (Color online) ZZ and XX components of the RKKY interaction as a function of impurity separation r, along (a) zigzag and (b) armchair directions. (c) DM component in the zigzag direction. The latter vanishes in the armchair direction. In all cases, the interaction amplitude decays as r^{-2}. The Fermi level $\epsilon_F \simeq -0.067$ crosses the uppermost K_τ valleys, without intersecting the valley at the Γ point, as indicated by the solid line in (d). (d) Schematic low-energy band structure for MoS_2 and WS_2, showing the spin inversion of the valence bands at K_1 and K_{-1} valleys. The black (red) curve corresponds to up (down) spin projection. The blue valley at Γ is quadratic and spin degenerate. Dashed and dotted lines indicate higher p-doping levels discussed in Fig. 3 and below.

where $\mathbf{s}(\mathbf{r}) = \frac{1}{2}\sum_i \delta(\mathbf{r} - \mathbf{r}_i)\boldsymbol{\sigma}_i$ represents the spin density for electron i ($\hbar = 1$), and $\mathbf{S}_j$ is the localized spin at site $\mathbf{R}_j$. For simplicity, we assume the same exchange coupling J for valence electrons on both d_{xy} and d_{z^2} Mo orbitals. One can treat H_{int} as a perturbation of H_0, obtaining at second order an effective interaction between the localized spins [35],

$$H_{\text{RKKY}} = J^2 \sum_{\alpha,\beta} S_1^\alpha \, \chi_{\alpha,\beta}(\mathbf{R}) \, S_2^\beta, \tag{4}$$

where $\chi_{\alpha,\beta}$ is the static spin susceptibility tensor of the electron gas, with α, β representing the Cartesian components, and $\mathbf{R}$ is the vector connecting the magnetic moments. The susceptibility can be calculated from the unperturbed real-space retarded Green's function [21,36],

$$\chi_{\alpha,\beta}(\mathbf{R}) = -\frac{1}{\pi}\,\text{Tr}\left[\int_{-\infty}^{\epsilon_F} d\epsilon \,\text{Im}\{\sigma_\alpha G(\mathbf{R},\epsilon^+)\sigma_\beta G(-\mathbf{R},\epsilon^+)\}\right], \tag{5}$$

where $\epsilon^+ = \epsilon + i0^+$, and σ are Pauli matrices for the spin degree of freedom. G stands for the 2×2 Green's-function matrix for the valence sector—processes that involve the conduction band are ignored, as they are strongly suppressed by the substantial energy gap. Different components of the susceptibility are $\chi_{\alpha,\beta}(\mathbf{R}) = -\frac{1}{\pi}\int_{-\infty}^{\epsilon_F} d\epsilon \,\text{Im} A_{\alpha,\beta}(\mathbf{R},\epsilon^+)$, with

$$A_{z,z} = \sum_s G_s(\mathbf{R},\epsilon^+)G_s(-\mathbf{R},\epsilon^+), \tag{6}$$

$$A_{x,x} = A_{y,y} = \sum_s G_s(\mathbf{R},\epsilon^+)G_{-s}(-\mathbf{R},\epsilon^+), \tag{7}$$

$$A_{x,y} = -A_{y,x} = -i\sum_s s\, G_s(\mathbf{R},\epsilon^+)G_{-s}(-\mathbf{R},\epsilon^+), \tag{8}$$

where $G_s(\mathbf{R},\epsilon^+) = G_\Gamma(\mathbf{R},\epsilon^+) + \sum_\tau G_{\tau,s}(\mathbf{R},\epsilon^+)$, and $s = \uparrow,\downarrow$. The effective anisotropic spin interaction between localized moments includes Ising (ZZ), XX, and Dzyaloshinskii-Moriya (DM) interactions, such that the RKKY Hamiltonian can be expressed as [21]

$$H_{\rm RKKY} = J_{XX}\left(S_1^x S_2^x + S_1^y S_2^y\right) + J_{ZZ} S_1^z S_2^z + J_{\rm DM}(\mathbf{S}_1 \times \mathbf{S}_2)_z, \quad (9)$$

where $J_{XX} = J^2\chi_{x,x}$, $J_{ZZ} = J^2\chi_{z,z}$, and $J_{\rm DM} = J^2\chi_{x,y}$. Notice that the XX and DM terms compete as to favor (anti)parallel or perpendicular alignment of the spins, respectively, in the xy plane at different impurity separations $\mathbf{R}$, creating, in general, an in-plane twisted spin structure, depending on their relative strength and sign.

It is convenient to obtain the Green's functions in momentum space and then Fourier transform back to real space (see Supplemental Material [37]). There are only two independent Green's functions at K_1 and K_{-1}, $g_{-1,-s}(\mathbf{R},\epsilon^+) = g_{1,s}(\mathbf{R},\epsilon^+)$. Omitting the energy variable for convenience, one obtains $G_s(\mathbf{R}) = G_\Gamma(R) + \sum_\tau e^{i\mathbf{K}_\tau\cdot\mathbf{R}} g_{\tau,s}(R)$, and using Eq. (6), we arrive at

$$\begin{aligned}{\rm Im}A_{z,z} = 2\big\{ & I_{G_\Gamma;G_\Gamma} + [\cos(\mathbf{K}_1\cdot\mathbf{R}) + \cos(\mathbf{K}_{-1}\cdot\mathbf{R})] \\ & \times \left(I_{G_\Gamma;g_{1,\uparrow}} + I_{G_\Gamma;g_{-1,\uparrow}}\right) + I_{g_{1,\uparrow};g_{1,\uparrow}} + I_{g_{-1,\uparrow};g_{-1,\uparrow}} \\ & + 2\cos[(\mathbf{K}_1 - \mathbf{K}_{-1})\cdot\mathbf{R}] I_{g_{1,\uparrow};g_{-1,\uparrow}}\big\}, \end{aligned} \quad (10)$$

where we have defined $I_{u;v}(\mathbf{R},\epsilon) \equiv {\rm Im}[u(\mathbf{R},\epsilon)v(\mathbf{R},\epsilon)]$ with $u,v = \{G_\Gamma; g_{1,\uparrow}; g_{-1,\uparrow}\}$. A similar procedure yields the $A_{x,x}$ and $A_{x,y}$ components. The cosines are angular coefficients that modulate the integral kernels $I_{u;v}$, depending on the relative direction of the impurities. An interesting feature of these expressions is that the underlying axial symmetries eliminate the DM (or XY) components for impurities arranged along armchair directions [37].

Fixed Fermi level. We define the dimensionless exchange interactions as $\bar{J}_i = -\frac{\Omega^2}{4\pi^3 J^2} J_i$, where $i = (ZZ, XX, {\rm DM})$, and Ω is the area of the first Brillouin zone. Let us first analyze the case in which the Fermi level does not intersect the Γ valley, i.e., with $-\epsilon_\Gamma < \epsilon_F < 0$, as indicated by the solid horizontal line in Fig. 2(d). $I_{g1,\uparrow;g1,\uparrow}$ is the only kernel contributing to the interaction. Figures 2(a) and 2(b) show the ZZ and XX components of the RKKY interaction vs impurity separation along the zigzag and armchair directions, respectively. The Fermi level is fixed at $\epsilon_F \simeq -0.067$, and $\bar{J}_i r^2$ is plotted as a function of the dimensionless distance r ($= R/a$), for large separations. The nearly constant amplitude reflects that the interaction decays as $1/r^2$. In the zigzag case, the XX angular coefficients are related by the sequence $\{1,-1/2,-1/2,\ldots\}$ with the ZZ ones (which are constant) [37], so that the ZZ component tends to dominate over the XX one. In the armchair direction, both ZZ and XX components coincide. Moreover, on sites in which $\int_{-\infty}^{\epsilon_F} d\epsilon\, I_{g_{1,\uparrow};g_{1,\uparrow}}(r,\epsilon)$ vanishes, both the ZZ and XX components vanish. Figure 2(c) shows the DM component in the zigzag direction, with a sequence $\{0,1,-1,\ldots\}$ with respect to ZZ. As mentioned, the symmetry of the lattice forces this component to vanish along the armchair direction.

In order to examine the spatial oscillations, it is convenient to define $q_{\pm 1}^F \equiv q_\pm(\epsilon_F)$ as the Fermi wave vector for the valleys with quantum numbers $\tau = \pm 1, s = \uparrow$ and $\tau = \mp 1, s = \downarrow$, and

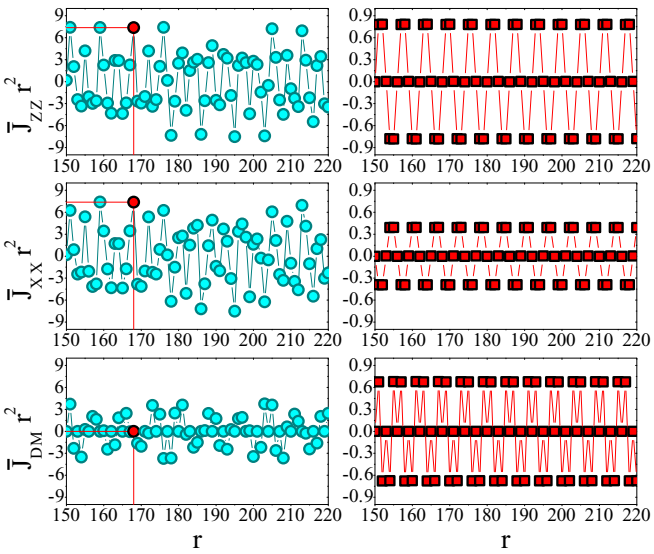

FIG. 3. (Color online) ZZ, XX, and DM components of the RKKY interaction as a function of separation in the zigzag direction. $\epsilon_F = -0.174$, as indicated by dashed line in Fig. 2(d). Left panels show the full interactions, including contributions of the Γ valley. The red horizontal and vertical lines indicate a fully isotropic interaction point. Right panels show the same quantities without including the Γ valley. Notice the different vertical scales.

$k_\Gamma^F \equiv k_\Gamma(\epsilon_F)$, the Fermi wave vector for the Γ valley. With $\epsilon_F = -0.067$, the modulation wavelength is $\Lambda \simeq 10$ in the zigzag direction, as observed in Figs. 2(a) and 2(c), and consistent with $\Lambda = \pi/q_1^F$. The modulation can be described by a sinusoidal function $\int_{-\infty}^{\epsilon_F} d\epsilon\, I_{g_{1,\uparrow};g_{1,\uparrow}}(r,\epsilon) \simeq c_1 r^{-2}\sin[2q_1^F r] = c_1 r^{-2}\sin[2\pi r/\Lambda]$. The amplitude here, $c_1 \simeq 0.45$, is nearly independent of the Fermi energy. Along the armchair direction, the modulation of the interimpurity interaction exhibits a more complex pattern, as observed in Fig. 2(b). Going from the zigzag to armchair directions amounts to replacing r by $\sqrt{3}r$, which can be seen as a shift of q_1^F to $\sqrt{3}q_1^F$ in the argument of the integral kernels [37], giving an effective k_F that is larger than in (and incommensurate with) the zigzag case. The incommensurate value also introduces aliasing effects.

Figure 3 shows results at $\epsilon_F \simeq -0.174$, such that the Fermi level intersects the band at the Γ point [dashed line in Fig. 2(d)], for impurities aligned along the zigzag direction. The right panels show the r dependence of the different interaction components, *without* the contribution of the Γ valley, while the left panels show the full interaction. The inclusion of the Γ valley not only significantly increases ($\times 10$) the amplitude of the modulation for all the interactions, but also produces a rather complex oscillatory pattern, due to the additional electron-scattering processes between states at Γ and K_τ points. The integral kernels contributing significantly in this regime are $I_{G_\Gamma;G_\Gamma}$, $I_{G_\Gamma;g_{1,\uparrow}}$, and $I_{g_{1,\uparrow};g_{1,\uparrow}}$ [37]. A sinusoidal fit gives $\int_{-\infty}^{\epsilon_F} d\epsilon\, I_{G_\Gamma;g_{1,\uparrow}} \simeq c_2 r^{-2}\sin([q_1^F + k_\Gamma^F]r)$, with a wavelength given by $\Lambda = 2\pi/[q_1^F + k_\Gamma^F] \simeq 4.92$, and $c_2 \simeq 0.24$; c_2 is found to be strongly dependent on the Fermi energy. In the limit $\epsilon_F \to -\epsilon_\Gamma$, the Γ to K_τ scattering processes produce an unusual spatial decay $r^{-5/2}$. However, the weight of this component is small compared to the ones

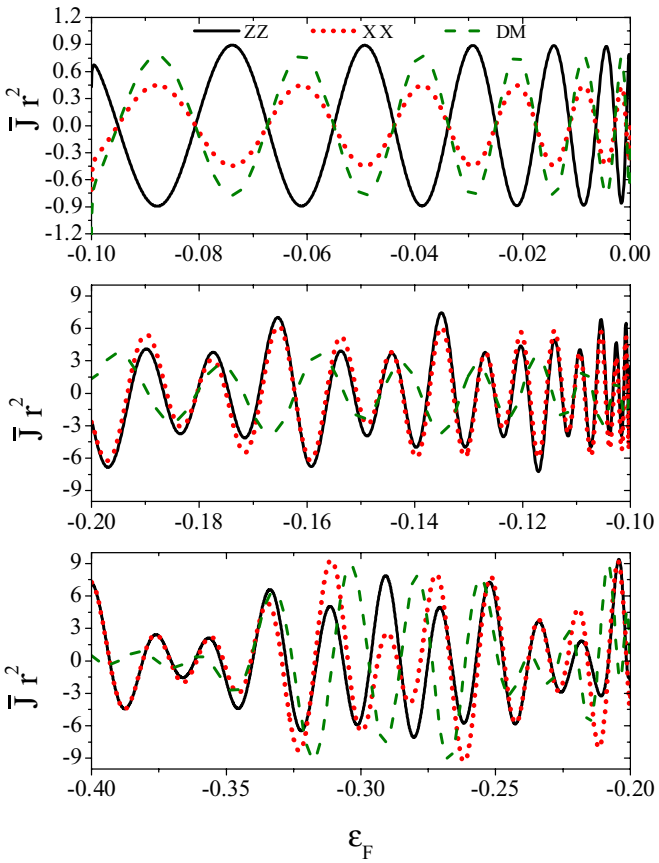

FIG. 4. (Color online) Comparison of the different components of the RKKY interaction for different Fermi energy regimes: (a) $-\epsilon_\Gamma < \epsilon_F < 0$, (b) $-2\lambda < \epsilon_F < -\epsilon_\Gamma$, and (c) $\epsilon_F < -2\lambda$. The interimpurity distance is fixed along the zigzag direction at $r = 50$. Notice different vertical scales.

in which the electronic processes take place within the same band valley, so that the expected r^{-2} decay dominates. Notice that the inclusion of the scattering processes at Γ allows for special impurity separations in which the DM term vanishes, and $J_{XX} = J_{ZZ} = J_{YY}$, rendering a fully isotropic exchange interaction between them (see, for example, $r = 168$ in the figure). This feature is a consequence of the spin degeneracy at this valley that effectively cancels the DM component. Similar features are observed for impurities separated along the armchair direction.

At higher p doping, $\epsilon_F < -2\lambda$ [dotted line in Fig. 2(d)], all valleys contribute to the indirect exchange, and the interaction exhibits very complex modulation patterns. The oscillations are dominated by $\int_{-\infty}^{\epsilon_F} d\epsilon\, I_{\Gamma;g_{-1,\uparrow}}(r,\epsilon) \simeq c_3 r^{-2} \sin([q_{-1}^F + k_\Gamma^F]r)$, $\int_{-\infty}^{\epsilon_F} d\epsilon\, I_{g_{1,\uparrow};g_{-1,\uparrow}}(r,\epsilon) \simeq c_4 r^{-2} \sin([q_1^F + q_{-1}^F]r)$, and $\int_{-\infty}^{\epsilon_F} d\epsilon\, I_{g_{-1,\uparrow};g_{-1,\uparrow}}(r,\epsilon) \simeq c_5 r^{-2} \sin[2q_{-1}^F r]$, where c_3 and c_4 depend strongly on ϵ_F, while c_5 is nearly independent of ϵ_F.

Fixed distance. We now analyze the case where the two impurities remain at a fixed distance along the zigzag direction, and analyze the RKKY interaction over a large Fermi energy range. We set $r = 50$ in the data shown below. For $-\epsilon_\Gamma < \epsilon_F < 0$, the Γ valley does not contribute to scattering [Fig. 4(a)]; all three components have similar amplitudes, with *XX* and DM oscillating in phase with each other, but out of phase with *ZZ*. This indicates an alternation between FM (AFM) in-plane order and AFM (FM) out-of-plane order as the energy is shifted. When the Fermi energy is positioned in the region $-2\lambda < \epsilon_F < -\epsilon_\Gamma$, shown in Fig. 4(b), the *ZZ* and *XX* interactions become in phase, while the DM modulation retains a longer period. This is caused by the absence of the term $I_{G_\Gamma;G_\Gamma}$ because the Γ valley is unaffected by the spin-orbit interaction. In this case, an isotropic exchange exists at particular values of ϵ_F for a vanishing DM component. At deeper Fermi energy $\epsilon_F < -2\lambda$, with all valleys contributing, one finds very interesting behavior: For $\epsilon_F \lesssim -0.35$, there exists another isotropic interaction regime with the *ZZ* and *XX* components contributing equally and the DM term weaker, or even zero.

Conclusions. We have shown that inclusion of the Γ valley, neglected in previous studies, changes predicted magnetic order for RKKY interacting impurities deposited on TMD materials. By judicious choice of impurity separation, level doping or gating, it is possible to alternate between isotropic and anisotropic order as well as to have well-defined (or not) in-plane order by manipulating the strength of the DM interaction. The results described above show behavior that can be readily tested by experiments, such as spin-polarized scanning tunneling microscopy [38,39]. Note that although we have focused on MoS_2, our results are applicable to other dichalcogenides, especially WS_2 that appears to be easier to dope (or gate). Characterization of the interaction between magnetic impurities with doping level would also provide an interesting but direct approach to determine the splitting of the Γ valley in real systems.

Acknowledgment. This work was supported in part by NSF Materials World Network Grant No. DMR-1108285.

[1] M. A. Ruderman and C. Kittel, Phys. Rev. **96**, 99 (1954).
[2] T. Kasuya, Prog. Theor. Phys. **16**, 45 (1956).
[3] K. Yosida, Phys. Rev. **106**, 893 (1957).
[4] P. Grünberg, R. Schreiber, Y. Pang, M. B. Brodsky, and H. Sowers, Phys. Rev. Lett. **57**, 2442 (1986).
[5] M. N. Baibich, J. M. Broto, A. Fert, F. Nguyen Van Dau, F. Petroff, P. Etienne, G. Creuzet, A. Friederich, and J. Chazelas, Phys. Rev. Lett. **61**, 2472 (1988).
[6] P. Bruno and C. Chappert, Phys. Rev. Lett. **67**, 1602 (1991).
[7] S. Wolf, A. Y. Chtchelkanova, and D. Treger, IBM J. Res. Dev. **50**, 101 (2006).
[8] B. Fischer and M. Klein, Phys. Rev. B **11**, 2025 (1975).
[9] V. K. Dugaev, V. I. Litvinov, and J. Barnas, Phys. Rev. B **74**, 224438 (2006).
[10] S. Saremi, Phys. Rev. B **76**, 184430 (2007).
[11] A. M. Black-Schaffer, Phys. Rev. B **81**, 205416 (2010).

[12] B. Uchoa, T. G. Rappoport, and A. H. Castro Neto, Phys. Rev. Lett. **106**, 016801 (2011).
[13] M. Sherafati and S. Satpathy, Phys. Rev. B **83**, 165425 (2011).
[14] M. Sherafati and S. Satpathy, Phys. Rev. B **84**, 125416 (2011).
[15] S. R. Power, F. S. M. Guimarães, A. T. Costa, R. B. Muniz, and M. S. Ferreira, Phys. Rev. B **85**, 195411 (2012).
[16] O. Roslyak, G. Gumbs, and D. Huang, J. Appl. Phys. **113**, 123702 (2013).
[17] E. Kogan, Graphene **02**, 8 (2013).
[18] S. Power and M. Ferreira, Crystals **3**, 49 (2013).
[19] K. S. Novoselov, D. Jiang, F. Schedin, T. J. Booth, V. V. Khotkevich, S. V. Morozov, and A. K. Geim, Proc. Natl. Acad. Sci. USA **102**, 10451 (2005).
[20] D. Xiao, G.-B. Liu, W. Feng, X. Xu, and W. Yao, Phys. Rev. Lett. **108**, 196802 (2012).
[21] F. Parhizgar, H. Rostami, and R. Asgari, Phys. Rev. B **87**, 125401 (2013).
[22] H. Hatami, T. Kernreiter, and U. Zülicke, Phys. Rev. B **90**, 045412 (2014).
[23] T. Cheiwchanchamnangij and W. R. L. Lambrecht, Phys. Rev. B **85**, 205302 (2012).
[24] W. S. Yun, S. W. Han, S. C. Hong, I. G. Kim, and J. D. Lee, Phys. Rev. B **85**, 033305 (2012).
[25] H. Shi, H. Pan, Y.-W. Zhang, and B. I. Yakobson, Phys. Rev. B **87**, 155304 (2013).
[26] A. Kormányos, V. Zólyomi, N. D. Drummond, P. Rakyta, G. Burkard, and V. I. Fal'ko, Phys. Rev. B **88**, 045416 (2013).
[27] F. Zahid, L. Liu, Y. Zhu, J. Wang, and H. Guo, AIP Adv. **3**, 052111 (2013).
[28] M. R. Laskar, D. N. Nath, L. Ma, E. W. Lee, C. H. Lee, T. Kent, Z. Yang, R. Mishra, M. A. Roldan, J.-C. Idrobo, S. T. Pantelides, S. J. Pennycook, R. C. Myers, Y. Wu, and S. Rajan, Appl. Phys. Lett. **104**, 092104 (2014).
[29] J. T. Ye, Y. J. Zhang, R. Akashi, M. S. Bahramy, R. Arita, and Y. Iwasa, Science **338**, 1193 (2012).
[30] Y. J. Zhang, J. T. Ye, Y. Yomogida, T. Takenobu, and Y. Iwasa, Nano Lett. **13**, 3023 (2013).
[31] D. Braga, I. Gutiérrez Lezama, H. Berger, and A. F. Morpurgo, Nano Lett. **12**, 5218 (2012).
[32] W. Sik Hwang, M. Remskar, R. Yan, V. Protasenko, K. Tahy, S. Doo Chae, H. (Grace) Xing, A. Seabaugh, and D. Jena, *70th Annual Device Research Conference (DRC), 2012* (IEEE, New York, 2012), pp. 187–188.
[33] S. Jo, N. Ubrig, H. Berger, A. B. Kuzmenko, and A. F. Morpurgo, Nano Lett. **14**, 2019 (2014).
[34] L. F. Mattheiss, Phys. Rev. B **8**, 3719 (1973).
[35] D. C. Mattis, *The Theory of Magnetism Made Simple* (World Scientific, Singapore, 2006).
[36] H. Imamura, P. Bruno, and Y. Utsumi, Phys. Rev. B **69**, 121303 (2004).
[37] See Supplemental Material at http://link.aps.org/supplemental/10.1103/PhysRevB.90.161403 for a detailed derivation of the RKKY interaction and angular dependences.
[38] L. Zhou, J. Wiebe, S. Lounis, E. Vedmedenko, F. Meier, S. Blügel, P. H. Dederichs, and R. Wiesendanger, Nat. Phys. **6**, 187 (2010).
[39] A. A. Khajetoorians, J. Wiebe, B. Chilian, S. Lounis, S. Blügel, and R. Wiesendanger, Nat. Phys. **8**, 497 (2012).